Research article

Bo Chen, Zhe He, Zhuo-Jun Liu, Yun-Kun Wang, Yu-Nan Gao, Igor Aharonovich, Zai-Quan Xu* and Jin Liu*

Simultaneously enhanced linear and nonlinear photon generations from WS_2 by using dielectric circular Bragg resonators

https://doi.org/10.1515/nanoph-2020-0143
Received February 24, 2020; accepted June 2, 2020

Abstract: Monolayer transition metal dichalcogenides (TMDs) have emerged as a promising platform for chip-integrated optoelectronics and non-linear optics. Here, we demonstrate a two-dimensional (2D) monolayer tungsten disulfide (WS_2) efficiently coupled to a dielectric circular Bragg resonator (CBR). The coupling of the WS_2 and CBR leads to pronounced enhancements in both photoluminescence (PL) and second harmonic generation (SHG) by a factor of 34 and 5, respectively. Our work provides a powerful tool to enhance the interactions between light and the 2D materials, paving the way for efficient on-chip optoelectronic devices.

Keywords: circular Bragg resonator; photoluminescence enhancement; second harmonic generation enhancement; tungsten disulfide.

***Corresponding authors: Zai-Quan Xu**, School of Mathematical and Physical Sciences, University of Technology Sydney, Ultimo 2007, NSW, Australia, E-mail: Zaiquan.Xu@uts.edu.au; and **Jin Liu**, State Key Laboratory of Optoelectronic Materials and Technologies, School of Physics, Sun Yat-sen University, Guangzhou 510275, China, E-mail: liujin23@mail.sysu.edu.cn

Bo Chen, Zhe He and Zhuo-Jun Liu: State Key Laboratory of Optoelectronic Materials and Technologies, School of Physics, Sun Yat-sen University, Guangzhou 510275, China. https://orcid.org/0000-0002-5039-0663 (B. Chen)

Yun-Kun Wang and Yu-Nan Gao: State Key Laboratory for Artificial Microstructure and Mesoscopic Physics, School of Physics, Peking University, Beijing 100871, China; Frontiers Science Center for Nano-optoelectronics, Beijing 100871, China

Igor Aharonovich: School of Mathematical and Physical Sciences, University of Technology Sydney, Ultimo 2007, NSW, Australia; ARC Centre of Excellence for Transformative Meta-Optical Systems, University of Technology Sydney, Ultimo, New South Wales, Australia.

1 Introduction

The monolayer transition metal dichalcogenides (TMDs) [1–5], such as MoS_2, $MoSe_2$, tungsten disulfide (WS_2) and WSe_2, are emerging platforms to study light–matter interaction at nanoscale. The exceptional optical properties, such as near-unity high quantum yield [6], nonblinking photon emission [7], valley polarization [8], stimulated emission [9], single-photon emission [10] and exciton–polariton emission [11], make them promising candidates for next-generation integrated optoelectronics [5]. Moreover, the monolayer TMDs have also exhibit superior performances in nonlinear optics [12]. A recent study on WS_2 has revealed large second-order nonlinear susceptibility due to the lack of central-symmetry [13, 14]. The second-order nonlinear susceptibility of pure WS_2 has been reported to be as large as 4.5 nm/V, several orders of magnitude larger than that of a conventional nonlinear crystal [13]. The giant nonlinear susceptibility together with the strong emission makes monolayer WS_2 an outstanding platform for frequency doubling, ultra-low threshold lasing and solar cells. However, the performances of atomically thin TMDs as light-emitting devices and non-linear optical materials are significantly limited by the weak light–matter interaction due to their atomic thickness.

The photonic waveguides [15, 16], optical fibers [17, 18], plasmonic structures [19–21] and microcavities [22–25] have been successfully demonstrated previously to manipulate the photon emission from TMDs. Among them, circular Bragg resonator (CBR) [26] features a small effective mode volume and can produce high photon extraction efficiency over a broad bandwidth. CBRs are straightforward to fabricate and have been widely employed to enhance the single-photon collection from quantum dots [27, 28] and nitrogen vacancy centers in diamond [29]. In addition, the CBRs have also been recently shown to be particularly attractive and promising for the integration with 2D materials [30].

Here, we demonstrate a monolayer WS_2 coupled to a silicon nitride (SiN) CBR. This hybrid system simultaneously experiences pronounced enhancements of both photoluminescence (PL) and second harmonic generation (SHG) at the CBR resonance when injecting low-power of green laser and high-power of near infrared laser, respectively. This work may offer a viable solution of building compact and efficient linear and nonlinear optoelectronic devices by the fusion between 2D material of integrated photonic devices.

2 Materials and methods

Within monolayer (1L) WS_2 crystal, as shown in Figure 1(a), sulfur (S) and tungsten (W) atoms are covalently bonded and alternatively arranged in a honeycomb structure. Monolayer WS_2 is a direct band gap material, exhibiting strong PL [4]. It also has a large second-order nonlinearity for the generation of SHG [13] owe to its non-centrosymmetric crystalline structure. A schematic in Figure 1(a) lower panel shows the operation mechanism of PL and SHG. In our experiment, monolayer WS_2 crystals were obtained by mechanically exfoliating its naturally occurring bulk crystalline counterpart using scotch tape and subsequently released onto a SiO_2/Si substrate [31]. The optical image of an exfoliated flake is shown in Figure 1(b), in which the dashed line highlights the monolayer WS_2. A fluorescent image of the flake, excited by ultra-violet (UV) light (A Tungsten-Halogen Lamp [400–2000 nm] filtered by a 450 nm cut-off short pass filter.), is shown in the inset, where the monolayer WS_2 exhibits significantly stronger intensity. The PL spectrum is collected from a home-built confocal microscope. A 532 nm continuous wave laser (~30 μW) is used to excite the WS_2 via a 50× air objective (numerical aperture, NA = 0.9). The PL spectrum is fitted with a Lorentzian model and is comprised of two components, i.e. neutral exciton and trion emission [32]. As shown in Figure 1(c), the PL spectrum consists of a strong neutral exciton emission centered at ~614 nm and a weak trion emission peaked at ~626 nm.

We design SiN (Si_3N_4) CBR structures to match the monolayer WS_2 emission. The resonator has a sub-micro disk surrounded by a few concentric rings, acting as antennas. The circular gratings operate under the second order Bragg condition and provide reflective feedback to the cavity, leading to near-vertical upward scattering of the photons, as schematically illustrated in Figure 2(a). Compared to the integrated photonic structures in literature [9, 22, 23, 33], the CBRs are easy to fabricate and can simultaneously enhance the spontaneous emission rate and improve the emission directionality to the free-space over a broad bandwidth. To get a suitable dimension of the CBR, we first simulate the intrinsic optical properties of the CBR. The simulated device consists of a 160 nm thick Si_3N_4 (n = 2.02), a 580 nm thick SiO_2 layer (n = 1.45) and a silicon substrate. The period and the filling faction are set to 375 and 100 nm, respectively, to meet the second-order Bragg condition. The calculated Purcell factors corresponding to the cavity resonances and the reflection band of 1D grating are presented in Figure 2(b). A clear resonance peak centered at 615 nm with a maximum Purcell factor of ~7 is shown when the central disk radius is 250 nm. The gratings also have a broadband reflection of up to 0.8. Using these parameters, we further construct 3D far-field intensity distribution by finite difference time domain (FDTD). Figure 2(c) plots the electric field profile within X-Y plane and more than 90% of the emissions are confined within an azimuthal angle of 20 degrees for the dipole on the CBR structure. Figure 2(d) shows the electric field profile of X-Z plane in logarithm scale for a CBR with a resonant wavelength of 615 nm which perfectly matches the emission wavelength of monolayer WS_2.

The CBR structures were patterned on SiN with standard electron-beam lithography (Raith Vistec EBPG5000 + 100 kV) followed by a reactive ion etching (RIE) system (Oxford PlasmaPro System100). The E-beam photoresist was removed by an oxygen plasma RIE process. After examining the CBR with a scanning electron beam (SEM), shown in Figure 2(e), we confirm the feature size of the CBR structure perfectly matches with our design. As shown in Figure 2(f), the cavity mode of CBR is visible at ~614.4 nm, consistent with the simulation results discussed above. The quality factor (Q) is ~180, defined as $Q = \lambda/\Delta\lambda$, where λ is the cavity resonance wavelength and $\Delta\lambda$ is the full-width at half-maximum (FWHM) of the resonance peak, respectively.

3 Enhanced PL

To enhance the PL of the monolayer WS_2, we then deterministically transferred it onto the center of fabricated CBR

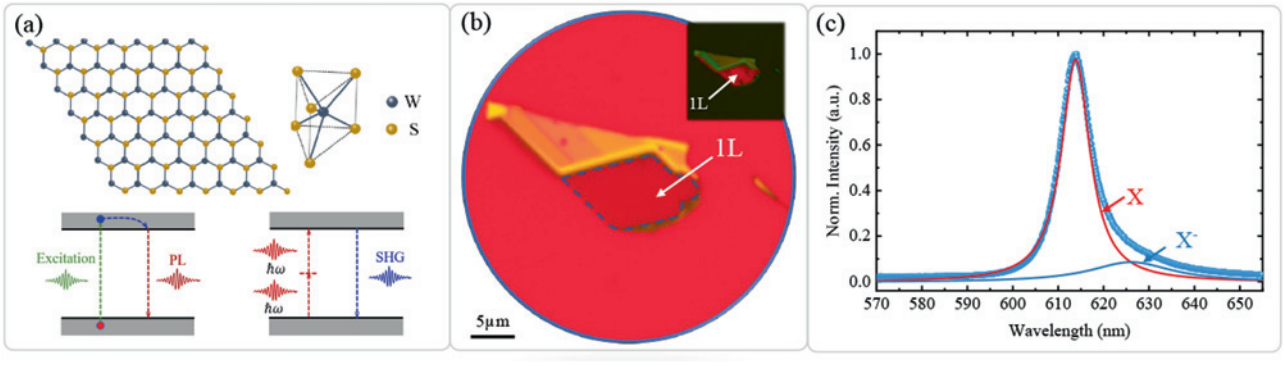

Figure 1: Optical characterizations of monolayer WS_2. (a) Schematic illustration of non-centrosymmetric monolayer WS_2 crystal lattice structure. (b) Optical image of a WS_2 mechanically exfoliated sample sitting on top of a SiO_2/Si substrate, dash line highlights the monolayer region. Scale bar: 5 μm. Inset: fluorescent image of the WS_2 flake. The red area in the inset, showing significantly brighter emission denotes the monolayer WS_2 emission illuminated by UV light. (c) Typical monolayer PL spectrum under 532 nm excitation showing a single strong neutral exciton emission centered at ~614 nm and a weak trion emission peaked at ~626 nm.

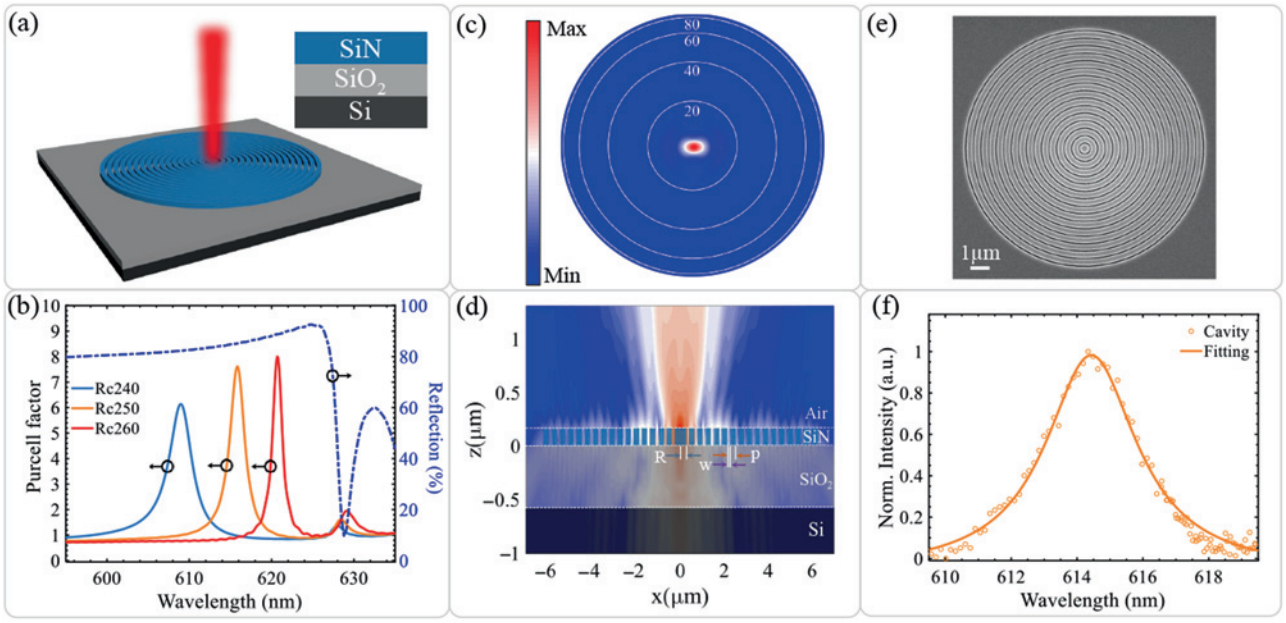

Figure 2: The design and the characterization of SiN CBRs. (a) A schematic illustration of the CBR. Inset: a schematic cross-sectional view of the substrate used to fabricate the CBRs. The simulated device consists of a 160 nm Si_3N_4 (n = 2.02), a 580 nm thick SiO_2 layer (n = 1.45) and a 500 μm thick Si. (b) Calculated Purcell factors for the CBRs with different cavity radius. The period and filling fraction are 375 and 100 nm, respectively. The blue dashed line denotes the reflection band of 1D grating structure. Lateral far-field (c) and vertical (d) intensity distribution at the cavity resonant wavelength of 615 nm. R, w and p denote the radius of the center disk, the filling fraction and the period, respectively. (e) SEM image of a fabricated CBR resonator. Scale bar: 1 μm. (f) The measured radiation spectrum of the CBR mode, showing a Q factor of ~180.

structure with an all-dry transfer technique [31]. In order to prevent the degradation of the material [34], monolayer WS_2 is encapsulated by hexagonal boron nitride (hBN) flakes. A schematic of the fabricated structure is shown in Figure 3(a) and the heterostructure is confirmed with an optical microscope. An optical image is shown in Figure 3(b), where the black dashed line outlines monolayer WS_2 and the white line defines hBN flakes, respectively. To evaluate the coupling of the WS_2 emission to the CBR, optical characterizations of the device were performed with a home-built scanning confocal microscope. As plotted in Figure 3(c), the PL spectrum collected from the center of the CBR at ambient condition shows two emission peaks located at 620.5 and 632.6 nm, which are attributed to the PL of neutral exciton and trion enhanced by the CBR mode, respectively. The PL emission and CBR resonant wavelength are red-shifted by ~6 and ~18 nm respectively after the transfer and introduction of hBN. We further measured the PL intensity over the CBR area, as shown in inset Figure 3(c), the emission are concentrated at the center of the CBR.

To maximize the coupling, we tune the PL and the cavity mode of CBR by changing the sample temperature [32, 35]. The normalized temperature-dependent PL spectra of the WS_2-CBR hybrid system are plotted in Figure 3(d). The PL emission and the CBR's resonance wavelength are highlighted with blue and purple dash lines, respectively. The PL spectrum starts to split into two peaks (trion and exciton) at 200 K. The trion peak shifts to 613 nm at 4 K. Meanwhile, the resonant wavelength of the cavity mode blue-shift from 632 nm at 300 K to 613 nm at 4 K as a result of the change of dielectric constant, which brings the trion emission into the resonance. As the tuning brings the emission line into the resonance with cavity mode, a 34 times emission enhancement is achieved. Figure 3(e) plots the PL for WS_2 on the center of CBR measured at 4 K, in which one great emission peak is observed at 613 nm. The emission is linear polarized, which is consistent with the polarization characteristic of the simulated cavity mode. Time-resolved PL measurements were carried out for the on-center and off-grating WS_2 using a 532 nm pulsed laser excitation (repetition rate 86 MHz, pulse width 12 ps) at 4 K and plotted in Figure 3(f). The fitted lifetime of the WS_2 on- and off-resonance is determined to be 24(2) and 47(3) ps, respectively, leading to a Purcell factor of ~2 for the WS_2 emission when coupled to the cavity.

4 Enhanced SHG

We further studied SHG once the WS_2 and CBR were coupled. SHG is a fundamental second-order nonlinear

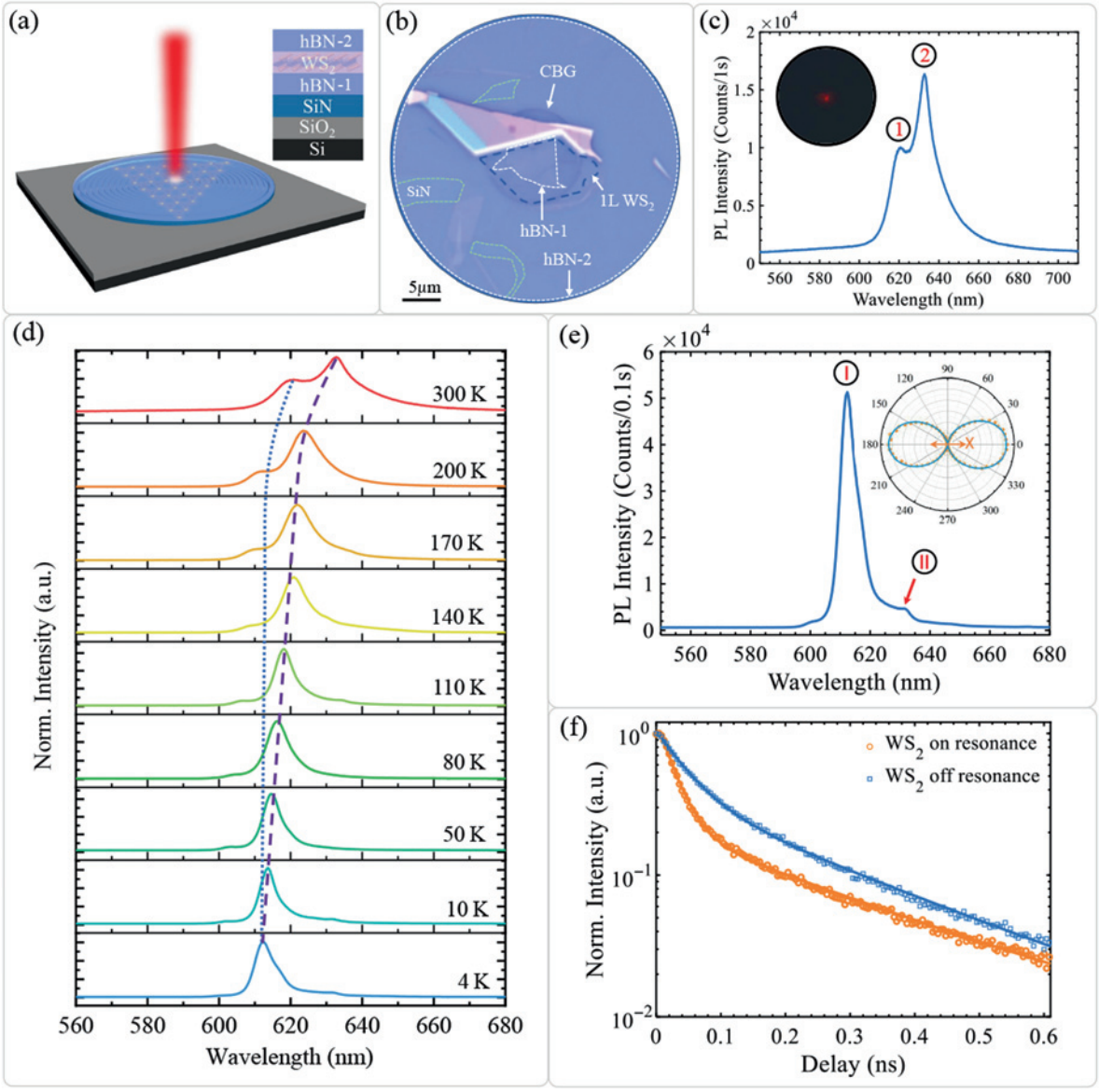

Figure 3: The characterization of the monolayer WS_2 coupled to SiN CBR. (a) Schematic diagram of the hBN-WS_2-hBN sandwich structure placed on the CBR. (b) Optical microscope image of the fabricated structure. The WS_2 and hBN layers are marked by black and white dashed lines, respectively. Scale bar: 5 μm. (c) The PL spectrum obtained from the center of the CBR at room temperature. Inset: optical micrograph of the PL intensity mapping over the area shown in (b). (d) PL emission of WS_2 on the center of the CBR structure measured from 300 to 4 K, the dot dashed line indicates the WS_2 and the long dashed line denotes the cavity mode. (e) The PL emission for WS_2 on the center of CBR measured at 4 K. The inset shows the polar plot of the PL (fixing the pumping at horizontal [*x*] polarization). (f) Time-resolved measurements for the WS_2 on-center and off-grating, revealing a ~2 times reduction of the radiative lifetime.

optical process, in which the frequency of the electromagnetic waves doubles by traveling through a nonlinear medium. The setup for measuring the SHG characteristics is schematically shown in Figure 4(a). Briefly, a tunable ps laser (~30 mW) was coupled onto the sample via a 50× objective. The SHG signal was filtered by a short-pass dichroic mirror and then passed by a half-wave plate and a polarizer before coupling into the CCD. Since the efficiency of grating in the spectrometer is polarization dependent, we rotated the half-wave plate instead of rotating the polarizer itself to analyze the polarization of SHG in our experiment. We fixed the excitation polarization to *x*-axis and scan the laser wavelength from 1214 to 1240 nm and collect signals from 607 to 620 nm. Figure 4(b) shows representative spectra of the fundamental signal (red line) and SHG signal (orange line), a clear emission at 613.5 nm

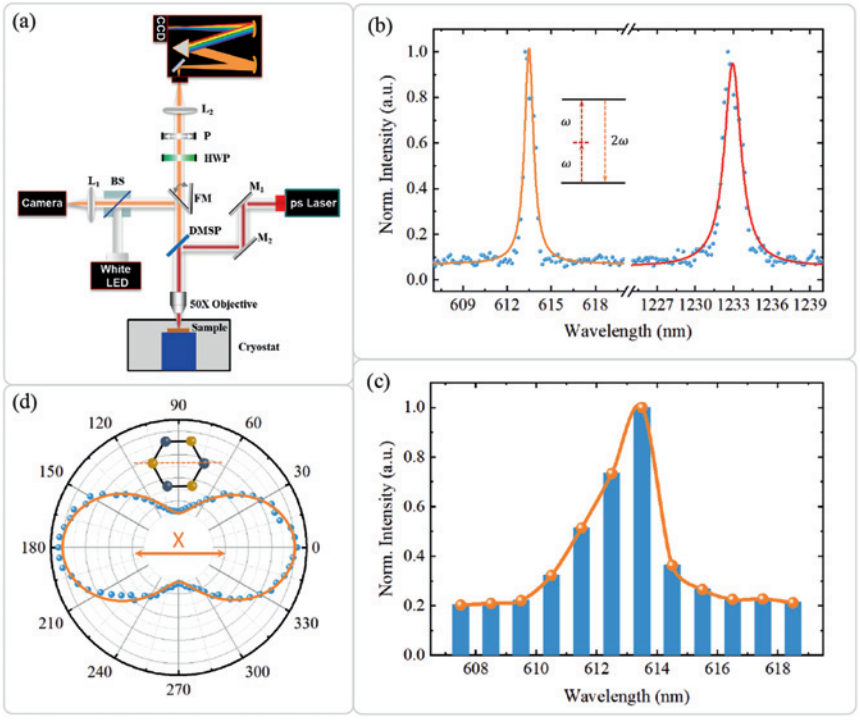

Figure 4: The characterization of the SHG enhancement for WS_2 coupled to CBR. (a) Schematic of the setup for SHG measurement. M_1, M_2: mirrors, FM: flip mirror, DMSP: shortpass dichroic mirror for 950 nm cutoff. BS: beam splitter, HWP: half-wave plate, P: polarizer, and L_1, L_2: lenses. (b) The normalized fundamental laser spectrum and a typical normalized spectrum of the SHG signal generated from a WS_2 monolayer at the CBR cavity mode. (c) The wavelength dependence of SHG by scanning the pumping wavelength at 4 K. (d) Polar plot of the measured intensity the SHG emission as a function of the detection angle for a given incident laser polarization (marked by the arrow).

(FWHM is 2.43 meV) is collected when the pumping is tuned to 1233 nm (FWHM is 5.18 meV), which is a clear evidence of the frequency doubling. The FWHM of the emission is 2.43 meV which is less than half of its excitation. We further compare the intensity of the SHG signal and a normalized intensity is plotted in Figure 4(c). The SHG signals reached the maximal values at the resonant wavelength and dramatically reduced on the off-resonant conditions. The on-resonance SHG signal (at ~613 nm) is over five times higher than the off-resonance which proves the enhancement due to the cavity resonance. The polarization dependent SHG is presented in Figure 4(d). The resonant SHG intensity is determined to be linearly polarized and is parallel to the polarization of the incident laser beam confirming that the SHG is governed by symmetry-breaking-induced nonlinearity in the monolayer WS_2 [36].

5 Conclusion

In summary, we have experimentally demonstrated enhancements of both PL and SHG on a single layered WS_2 coupled to a SiN CBR. Approximately a 34 fold of PL enhancement and a 5 times enhancement in SHG are achieved when the coupling is realized. The higher PL enhancement is attributed to the enhanced emission rate (Purcell effect) and the stronger trion emission at cryogenic temperature. The temperature-dependent emission measurement reveals the operation mechanism of the enhancement and offers a strategy that can be applied to hybrid 2D photonics systems. Our results provide a powerful tool for creating compact and efficient optoelectronic devices for future on-chip nanophotonics and nonlinear optics.

Acknowledgment: We acknowledge the Fundamental Research Funds for the Central Universities and the national supercomputer center in Guangzhou. National Key R&D Program of China (2018YFA0306100); National Natural Science Foundation of China (11874437, 61935009); Guangzhou Science and Technology Project (201805010004); Natural Science Foundation of Guangdong (2018B030311027, 2016A030306016, 2016TQ03X981).

Research funding: This work supported by the National Key R&D Program of China (2018YFA0306100); National Natural Science Foundation of China (11874437, 61935009); Guangzhou Science and Technology Project (201805010004); Natural Science Foundation of Guangdong (2018B030311027, 2016A030306016, 2016TQ03X981).

Author contribution: All the authors have accepted responsibility for the entire content of this submitted manuscript and approved submission.

Conflict of interest statement: The authors declare no conflicts of interest regarding this article.

References

[1] A. Splendiani, L. Sun, Y. Zhang, et al., "Emerging photoluminescence in monolayer MoS_2," *Nano Lett.*, vol. 10, p. 1271, 2010.

[2] W. Zhao, Z. Ghorannevis, L. Chu, et al., "Evolution of electronic structure in atomically thin sheets of WS_2 and WSe_2," *ACS Nano*, vol. 7, p. 791, 2012.

[3] Y. H. Chang, W. Zhang, Y. Zhu, et al., "Monolayer $MoSe_2$ grown by chemical vapor deposition for fast photodetection," *ACS Nano*, vol. 8, p. 8582, 2014.

[4] H. R. Gutiérrez, N. Perea-López, A. L. Elías, et al., "Extraordinary room-temperature photoluminescence in triangular WS_2 monolayers," *Nano Lett.*, vol. 13, p. 3447, 2013.

[5] Q. H. Wang, K. Kalantar-Zadeh, A. Kis, J. N. Coleman, and M. S. Strano, "Electronics and optoelectronics of two-dimensional transition metal dichalcogenides," *Nat. Nanotechnol.*, vol. 7, p. 699, 2012.

[6] L. Yuan, and L. Huang, "Exciton dynamics and annihilation in WS_2 2D semiconductors," *Nanoscale*, vol. 7, p. 7402, 2015.

[7] N. Peimyoo, J. Shang, C. Cong, et al., "Nonblinking, intense two-dimensional light emitter: Monolayer WS_2 triangles," *ACS Nano*, vol. 7, p. 10985, 2013.

[8] S. H. Gong, F. Alpeggiani, B. Sciacca, E. C. Garnett, and L. Kuipers, "Nanoscale chiral valley-photon interface through optical spin-orbit coupling," *Science*, vol. 359, p. 443, 2018.

[9] Y. Ye, Z. J. Wong, X. Lu, et al., "Monolayer excitonic laser," *Nat. Photonics*, vol. 9, p. 733, 2015.

[10] C. Palacios-Berraquero, D. M. Kara, A. R. P. Montblanch, et al., "Large-scale quantum-emitter arrays in atomically thin semiconductors," *Nat. Commun.*, vol. 8, p. 1, 2017.

[11] L. C. Flatten, Z. He, D. M. Coles, et al., "Room-temperature exciton-polaritons with two-dimensional WS_2," *Sci. Rep.*, vol. 6, p. 33134, 2016.

[12] Y. R. Shen, "Surface properties probed by second-harmonic and sum-frequency generation," *Nature*, vol. 337, p. 519, 1989.

[13] C. Janisch, Y. Wang, D. Ma, et al., "Extraordinary second harmonic generation in tungsten disulfide monolayers," *Sci. Rep.*, vol. 4, p. 5530, 2014.

[14] H. Zeng, G. B. Liu, J. Dai, et al., "Optical signature of symmetry variations and spin-valley coupling in atomically thin tungsten dichalcogenides," *Sci. Rep.*, vol. 3, p. 1608, 2013.

[15] H. Chen, V. Corboliou, A. S. Solntsev, et al., "Enhanced second-harmonic generation from two-dimensional $MoSe_2$ on a silicon waveguide," *Light Sci. Appl.*, vol. 6, 2017, Art no.e17060.

[16] P. Tonndorf, O. Del Pozo-Zamudio, N. Gruhler, et al., "On-chip waveguide coupling of a layered semiconductor single-photon source," *Nano. Lett.*, vol. 17, p. 5446, 2017.

[17] A. W. Schell, H. Takashima, T. T. Tran, I. Aharonovich, and S. Takeuchi, "Coupling quantum emitters in 2D materials with tapered fibers," *ACS Photonics*, vol. 4, p. 761, 2017.

[18] J. H. Chen, J. Tan, G. X. Wu, X. J. Zhang, F. Xu, and Y. Q. Lu, "Tunable and enhanced light emission in hybrid WS_2-optical-fiber-nanowire structures," *Light Sci. Appl.*, vol. 8, p. 1, 2019.

[19] S. Najmaei, A. Mlayah, A. Arbouet, C. Girard, J. Leotin, and J. Lou, "Plasmonic pumping of excitonic photoluminescence in hybrid MoS_2-Au nanostructures," *ACS Nano*, vol. 8, p. 12682, 2014.

[20] Y. Kang, S. Najmaei, Z. Liu, et al., "Plasmonic hot electron induced structural phase transition in a MoS_2 monolayer," *Adv. Mater.*, vol. 26, p. 6467, 2014.

[21] Z. Wang, Z. Dong, Y. Gu, et al., "Giant photoluminescence enhancement in tungsten-diselenide-gold plasmonic hybrid structures," *Nat. Commun.*, vol. 7, p. 11283, 2016.

[22] X. Liu, T. Galfsky, Z. Sun, et al., "Strong light-matter coupling in two-dimensional atomic crystals," *Nat. Photonics*, vol. 9, p. 30, 2015.

[23] S. Wu, S. Buckley, J. R. Schaibley, et al., "Monolayer semiconductor nanocavity lasers with ultralow thresholds," *Nature*, vol. 520, p. 69, 2015.

[24] Y. Li, J. Zhang, D. Huang, et al., "Room-temperature continuous-wave lasing from monolayer molybdenum ditelluride integrated with a silicon nanobeam cavity," *Nat. Nanotechnol.*, vol. 12, p. 987, 2017.

[25] L. Fang, Q. Yuan, H. Fang, et al., "Multiple optical frequency conversions in few–layer GaSe assisted by a photonic crystal cavity," *Adv. Opt. Mater.*, vol. 6, p. 1800698, 2018.

[26] M. Y. Su, and R. P. Mirin, "Enhanced light extraction from circular Bragg grating coupled microcavities," *Appl. Phys. Lett.*, vol. 89, 2006, Art no.033105.

[27] L. Sapienza, M. Davanço, A. Badolato, and K. Srinivasan, "Nanoscale optical positioning of single quantum dots for bright and pure single-photon emission," *Nat. Commun.*, vol. 6, p. 1, 2015.

[28] J. Liu, R. Su, Y. Wei, et al., "A solid-state source of strongly entangled photon pairs with high brightness and indistinguishability," *Nat Nanotechnol.*, vol. 14, p. 586, 2019.

[29] L. Li, E. H. Chen, J. Zheng, et al., "Efficient photon collection from a nitrogen vacancy center in a circular bullseye grating," *Nano Lett.*, vol. 15, p. 1493, 2015.

[30] N. M. H. Duong, Z. Q. Xu, M. Kianinia, et al., "Enhanced emission from WSe_2 monolayers coupled to circular Bragg gratings," *ACS Photonics*, vol. 5, p. 3950, 2018.

[31] A. Castellanos-Gomez, M. Buscema, R. Molenaar, et al., "Deterministic transfer of two-dimensional materials by all-dry viscoelastic stamping," *2D Mater.*, vol. 1, 2014, Art no.011002.

[32] Y. Kobayashi, S. Sasaki, S. Mori, et al., "Growth and optical properties of high-quality monolayer WS_2 on graphite," *ACS Nano*, vol. 9, p. 4056, 2015.

[33] R. Su, S. Liu, Y. Wei, et al., "Bright and pure single-photons from quantum dots in micropillar cavities under up-converted excitation," *Sci. Bull.*, vol. 63, p. 739, 2018.

[34] M. W. Iqbal, M. Z. Iqbal, M. F. Khan, et al., "High-mobility and air-stable single-layer WS_2 field-effect transistors sandwiched between chemical vapor deposition-grown hexagonal BN films," *Sci. Rep.*, vol. 5, p. 10699, 2015.

[35] M. T., and D. J. Late, "Temperature dependent phonon shifts in single-layer WS_2," *ACS Appl. Mater. Interfaces*, vol. 6, p. 1158, 2014.

[36] X. Fan, Y. Jiang, X. Zhuang, et al., "Broken symmetry induced strong nonlinear optical effects in spiral WS_2 nanosheets," *ACS Nano*, vol. 11, p. 4892, 2017.